JMEPEG
https://doi.org/10.1007/s11665-024-09258-0

1059-9495/$19.00

ORIGINAL RESEARCH ARTICLE

Refinement of Primary Si in Hypereutectic Al-Si Alloy by Serpentine Channel with Spoiler

Dong Wang, Cuncai Jiang, Gangyi Cai, Jun Li, Yanbo Hui, Yonggang Guo, and Fahai Ba

Submitted: 7 July 2023 / Revised: 9 January 2024 / Accepted: 17 January 2024

The microstructure and mechanical properties of hypereutectic Ai-Si alloys prepared by serpentine channel with spoiler were investigated. The flow state of the melt during the slurry preparation by the serpentine channel was simulated. The Al-Si alloy with the spoiler was superior to that without the spoiler at identical pouring conditions. The microstructure of the hypereutectic Ai-Si alloy was composed of the primary Si and Al-Si eutectic phases. The flow direction of the alloy slurry was disorganized because of the stirring effect of the spoiler, which improved the nuclei exfoliation and spherical growth of the primary Si. The spoiler refined the primary Si grains, and enhanced the mechanical properties of the Al-Si alloy. As the pouring temperature decreased from 746 to 701 °C, the size of the primary Si grains gradually decreased, and the tensile strength of the Al-Si alloy increased. The equivalent diameter of the primary Si grains could be reduced to 21.2 μm, and the tensile strength could be increased to 298 MPa under a pouring temperature of 701 °C.

Keywords aluminum, casting and solidification, primary Si, refinement, serpentine channel

1. Introduction

The hypereutectic Al-Si alloy has been widely used for making heat-resistant parts such as engine blocks and automobile pistons due to its excellent mechanical properties, corrosion resistance and high strength-to-weight ratio (Ref 1–3). The as-cast microstructure of the hypereutectic Al-Si alloy is composed of primary Si and eutectic phase, and the size and morphology of the primary Si dominate the mechanical properties of the hypereutectic Al-Si alloy (Ref 4). The primary Si always shows polygonal or lath shape during solidification for the hypereutectic Al-Si alloy prepared by the conventional casting process, and its equivalent diameter is even larger than 150 μm (Ref 5). These large-size primary Si grains with an irregular shape will be detrimental to the mechanical properties of the hypereutectic Al-Si alloy (Ref 6, 7). Therefore, the refinement of primary Si grains in the hypereutectic Al-Si alloy has been a constant topic of interest.

The semi-solid process has been considered as a potential processing technique. So far, the primary Si grains in the semi-solid slurry have been refined by a variety of methods, such as the elemental modification (Ref 2, 8), electromagnetic stirring (Ref 9, 10), wavelike sloping plate rheocasting (Ref 11), and cooling slope casting (Ref 12, 13). The phosphorus modifier increased the nucleation rate of the primary Si, and refined its grains in the hypereutectic Al-Si alloy (Ref 8). It is worth noting that the alloy composition was changed by the modifier, and the mechanical properties of the alloy needed to be reassessed. The primary Si grains were refined by the electromagnetic stirring technology because of the mechanical interaction between the primary Si and the surrounding molten metals (Ref 9). The primary phase in Ai-Si-Mg alloy could be effectively refined by the cooling slope casting because a high undercooling increased the nucleation rate of the primary phase in the alloy slurry (Ref 12). However, the above methods often employed a single pathway to refine the primary Si grains, and the refining performance was limited.

Serpentine channel has been proposed to refine the primary phase in the Al-Si alloy (Ref 14, 15). Serpentine channel inner wall had the cooling and stirring effects on the Al-Si alloy melt during the pouring process, which increased the nucleation rate of the primary Si in the Al-Si alloy melt (Ref 16). Thus, the serpentine channel pouring was an effective approach for the refinement of the primary Si in the hypereutectic Al-Si alloy. Compared to the graphite channel, the copper channel exhibited an excellent grain refining ability due to its high thermal conductivity (Ref 18). The pouring temperature also played a vital role in the size and morphology of the primary Si grains in the hypereutectic Al-Si alloy slurry (Ref 19). The equivalent diameter of the primary Si grains in the Al-20 wt.% Si alloy decreased from 34 to 25 μm by increasing the number of channel curves (Ref 17). However, the refining performance of the serpentine channel on the primary Si grains was still limited by its smooth inner wall. Fortunately, the turbulent flow, which was generated by wavelike sloping plate, resulted in massive fracture of the primary Si grains in the Al-Si alloy melt (Ref 11). It will be interesting to investigate the effect of this

Dong Wang and **Cuncai Jiang**, School of Mechanical and Electrical Engineering, Henan University of Technology, Zhengzhou 450001, China; and Henan Provincial Engineering Research Centre of Automotive Composite Materials, Zhengzhou 450001, China; **Gangyi Cai, Jun Li, Yanbo Hui,** and **Yonggang Guo**, School of Mechanical and Electrical Engineering, Henan University of Technology, Zhengzhou 450001, China; and **Fahai Ba**, Shanghai Research Institute of Materials Co., Shanghai 200433, China. Contact e-mails: wangdong23322@126.com, huiyb@haut.edu.cn, and nanogyg@163.com.

Published online: 26 February 2024

wavelike protrusion on the primary Si in the hypereutectic Al-Si alloy prepared by the serpentine channel.

In the present work, a novel structure of serpentine channel with spoilers is proposed to refine the primary Si grains in the hypereutectic Al-Si alloy slurry. The aim of the present work is to verify the feasibility of this structure by analyzing the microstructure and mechanical properties of the Al-Si alloy. To do this, the pouring temperature was experimentally optimized. The favorable effect of the spoiler on the size of the primary Si grains was investigated by comparing the Al-Si alloy prepared with and without spoiler. With help of the microstructural characterization and finite element analysis, the refinement mechanism of the primary Si was discussed in consideration of the stirring effect of the spoilers on the Al-Si semi-solid alloy slurry.

2. Materials and Methods

The Al-20%Si alloy in this study was prepared using an Al-50%Si master alloy (50%, all compositions quoted in this work were in wt.%) and pure aluminium (purity: 99.9%) in a resistance furnace, and its chemical composition is shown in Table 1. The liquidus and solidus temperatures of the Al-20%Si alloy were 690.8 and 480.2 °C, respectively, as measured by differential scanning calorimetry (Fig. 1). A cylindrical steel (Q235) crucible was used to collect the alloy slurry in the furnace, of which the dimension was Φ80 × 120 mm with a thickness of 5 mm. The slurry temperature was monitored by using a K-type thermocouple with an accuracy of ± 0.1 °C. In order to ensure the same cooling rate, each cast ingot was weighed to be 2.0 ± 0.1 kg.

Table 1 Chemical compositions of the Al-20%Si used in this study (wt.%)

Si	Mg	Cu	Mn	Cr	Zn	Fe	Ni	Al
20.23	0.52	3.19	0.01	0.02	0.02	0.15	0.01	Bal.

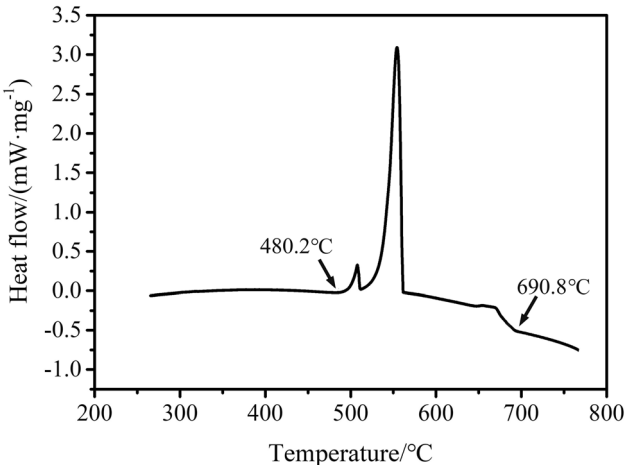

Fig. 1 DSC curve of Al-20%Si alloy obtained during solidification process

Figure 2 presents the integral structure of the serpentine channel with the spoilers, which is composed of four-curve copper channel. The materials of both the serpentine channel and the spoilers were pure copper. Half-cylindrical serpentine channel with a diameter of 30 mm, of which every segment was 106 mm long with 90° included angle and 30 mm curvature radius at the bends, was machined in the middle of a copper plate of 406 × 180 × 30 mm, and the other half was machined in the same dimensions. The projection of the spoiler with a tilt angle of 60° was a bow shape, of which the radius was 15 mm with a center angle of 120°. The spoilers were installed on the inner wall of the serpentine channel through pins, and the installation positions of the spoilers were located at the trisection point between two adjacent bends. Firstly, the Al-Si alloy melt in graphite crucible was heated to 800-820 °C by an electrical resistance furnace, which was about 60 °C higher than the highest pouring temperature. Then, the slurry was stirred and cooled to the chosen pouring temperature. The slurry pouring temperature was set at 761 °C (Alloy O), 746 °C (Alloy I), 731 °C (Alloy II), 716 °C (Alloy III), 701 °C (Alloy IV) and 686 °C (Alloy V), respectively. Secondly, the slurry was poured through the serpentine channel with the spoilers, and then dumped into a collection crucible. Finally, the slurry was rapidly quenched in cold water to reserve the semisolid slurry microstructure. For comparison, the Al-Si alloy slurry was poured directly into the collection crucible and through the serpentine channel without the spoilers at 701 °C, respectively.

The specimens for microstructure examination and tensile tests were prepared by wire cutting across the quenched alloy. After grinding and polishing, the specimens were etched with a C_2H_5OH-0.5% HF reagent for 20 s to reveal the microstructure of the specimens. The alloy was characterized by using an x-ray diffractometer (Smart Lab) at a stepwise of 0.1°, and the phases of the alloy were identified by Jade5.0 software. The microstructural examination was made using a Neuphoto21 optical microscope. The equivalent diameters of the primary Si grains were calculated using an image-analysis software (Image

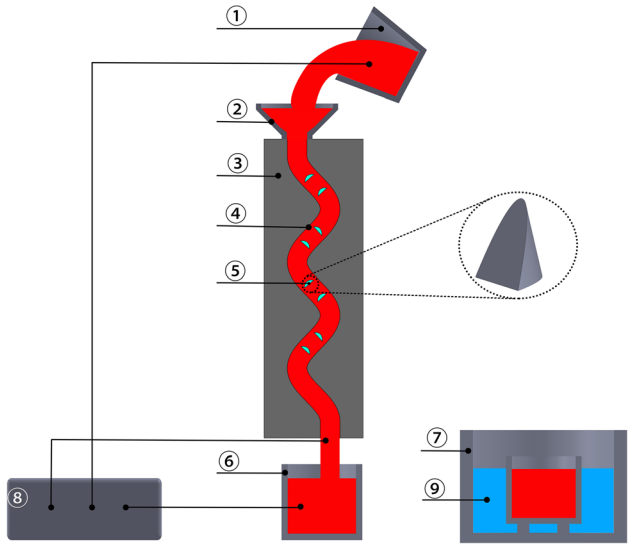

Fig. 2 Schematic diagram of the copper serpentine channel with the spoilers. ① Melting crucible, ② Pouring cup, ③ Copper mold, ④ Serpentine channel, ⑤ Spoiler, ⑥ Collection crucible, ⑦ Cooling box, ⑧ Thermocouple, ⑨ Cooling water

Pro Plus). The shape coefficient *Fs* of the primary Si grains was calculated using Eq 1 (Ref 16):

$$F_s = \frac{N}{\sum_{i=1}^{N} \frac{P_i^2}{4\pi A_i}} \quad \text{(Eq 1)}$$

where A, N, and P was the equivalent area, the number and the perimeter of the primary Si grains in one view, respectively.

To obtain a statistical average of the equivalent diameter and shape coefficient of the primary Si grains, three samples were taken along the radial direction of the cast ingot, and three views were randomly selected from each sample. Tensile tests were implemented at room temperature using a testing machine (Zwick/Roell Z020) at a loading rate of 0.2 mm/min. The ultimate tensile strength was obtained directly from the stress-strain curve, and calculated from the mean of three tests.

The ANSYS Fluent 19.2 software was employed to simulate the fluid flow of the alloy slurry in the serpentine channel. The materials of the channel wall and slurry selected during simulation were pure copper and Al, respectively. At the inlet of the channel, the pouring temperature of the slurry was set as 701 °C, and the velocity was set as 10 m/s. The outlet of the channel was exposed to atmosphere. The fluid flow in the serpentine channel was assumed as the turbulent flow according to the Reynolds number. The Reynolds number was defined using Eq 2 (Ref 20, 21):

$$R_e = \frac{\rho U L}{\mu} \quad \text{(Eq 2)}$$

where U was the velocity at the inlet, L was the hydraulic diameter which represented the serpentine channel diameter, ρ was the density of the slurry (2.38 g/mm^3), and μ represented the viscosity coefficient of the slurry.

3. Results

3.1 Microstructure and Mechanical Properties of the Semi-Solid Al-20%Si Alloy

Figure 3(a) depicts the typical microstructure of the semi-solid Al-20%Si alloy slurry poured directly into the collection crucible at 701 °C. The microstructure was composed of an irregular eutectic structure containing the primary phase and eutectic phase. With the help of XRD analysis in Fig. 3(b), the primary phase matched the Si grains, and the dendritic phase corresponded to Al-Si eutectic phase. The primary Si grains in the solidified Al-20%Si alloy exhibited a plate-like shape, and the average shape coefficient is 0.63. The solidification mode of the Al-Si eutectic phase was dendrite growth surrounding the primary Si grains, as shown in Fig. 3(a). The average equivalent diameter of the primary Si grains was 82.6 μm, and the maximum diameter of the primary Si grain approached to 150 μm.

In order to study the effect of the spoilers on the microstructure of the Al-20%Si alloy, a set of comparative tests were carried out under identical conditions. Figure 4(a) shows the microstructure of the semi-solid Al-20%Si alloy slurry fabricated by the serpentine channel without the spoilers. The primary Si grains distributed uniformly in the alloy microstructure. The average equivalent diameter of these primary Si grains is 24.8 μm, which is less than that of the traditional solidified Al-20%Si alloy in Fig. 3(a). Plenty of elliptical primary Si grains were formed in the Al-Si alloy slurry, and the average shape coefficient of the primary Si is 0.81. When the spoilers were applied to the serpentine channel, a large number of fine primary Si grains appeared in the Al-20%Si alloy slurry microstructure (Fig. 4b). The size of the primary Si grains further decreased compared to that prepared without the spoilers, and the average equivalent diameter of the primary Si grains is 21.2 μm. The morphology of the primary Si grains in the semi-solid slurry was mainly in an elliptic shape by introducing the spoilers. Nevertheless, the distribution uniformity of the primary Si grains seemed unchangeable compared to that prepared without the spoilers.

The tensile stress-strain curves of the Al-20%Si alloy prepared by the serpentine channel with/without the spoilers under the pouring temperature of 701 °C are shown in Fig. 5. Both curves went through an initial elastic deformation, and following with a rapid stress drop. It could be found that plastic elongation rate of $> 9\%$ was obtained before the rapid stress drop, suggesting ductile nature of the alloy. Compared to the alloy without the spoilers, the plastic elongation rate of the alloy with the spoilers tended to enlarge. The tensile strength, corresponding to the ultimate stress, was directly determined from the stress-strain curves. The tensile strength of the alloy with the spoilers was 298 MPa, which was higher than 255 MPa for the alloy prepared without the spoilers.

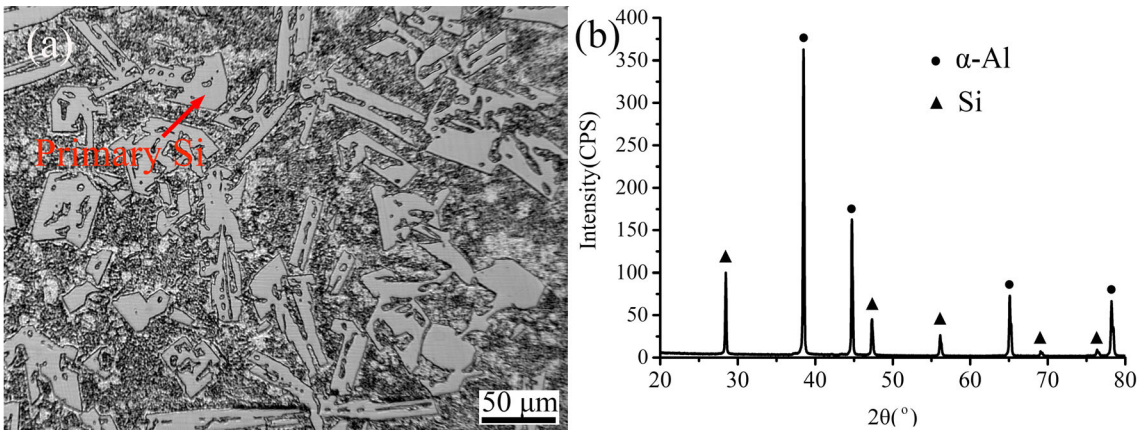

Fig. 3 (a) Microstructure of traditional solidified Al-20%Si alloy poured at 701 °C, (b) XRD pattern taken from the Al-20 %Si alloy

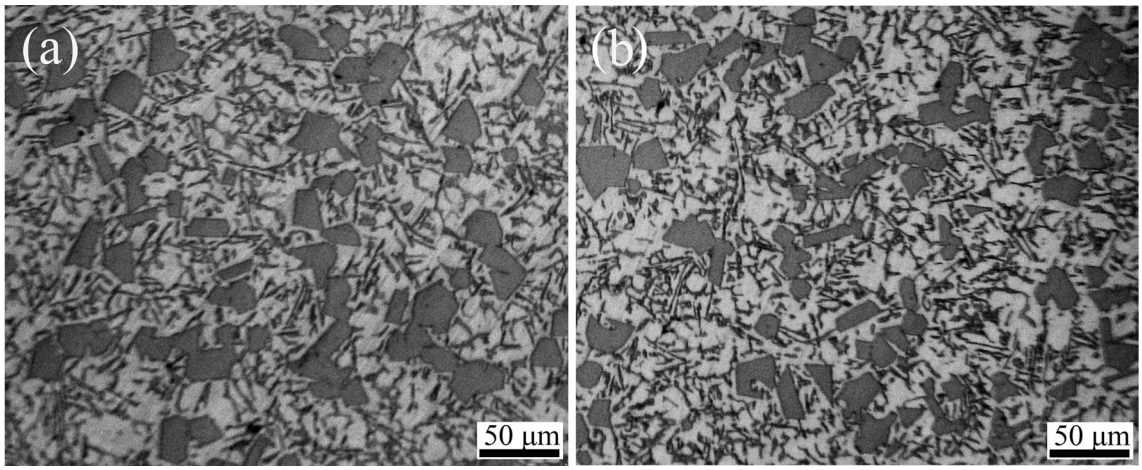

Fig. 4 Microstructure of the Al-20%Si alloy prepared by the serpentine channel under the pouring temperature of 701 °C, (a) without the spoilers, (b) with the spoilers

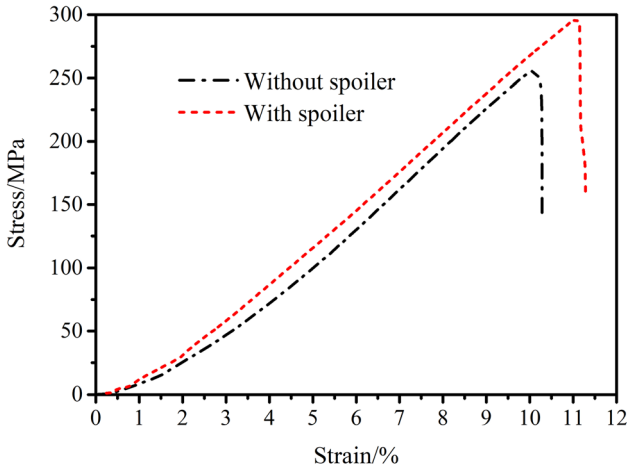

Fig. 5 Tensile stress-strain curves of the Al-20%Si alloy prepared by the serpentine channel with and without the spoilers under the pouring temperature of 701 °C

Table 2 The outlet temperature and solidified shell weight of the Al-20%Si slurry under different pouring temperatures

Pouring temperature, °C	Outlet temperature, °C	Weight of solidified shell, g
761	696	26.8
746	678	45.3
731	666	63.2
716	650	76.4
701	637	101.6
686	…	249.2

3.2 Effect of Pouring Temperature on the Microstructure and Mechanical Properties

To optimize the pouring temperature, it was necessary to investigate the effect of the pouring temperature on the size of the primary Si grains. In this study, six different temperatures were applied in the pouring process of the Al-20%Si alloy slurry. The outlet temperatures and the weight of the solidified shells of the Al-Si alloy slurry prepared under different pouring temperatures are shown in Table 2. The outlet temperature of the alloy slurry under the pouring temperature of 761 °C was 696 °C, which was higher than the liquidus temperature of the alloy. In this case, the alloy slurry in the serpentine channel was liquid. The outlet temperatures of the alloy slurry under the pouring temperature of 701-746 °C lay between the solidus and the liquidus temperatures of the Al-20%Si alloy. However, the outlet temperature of the alloy slurry under the pouring temperature of 686 °C was not measured because the serpentine channel was blocked by the slurry. The solidified shell weight of the slurry increased gradually when the pouring temperature decreased. This result indicated that the pouring temperature had an important effect on the solidified shell formed in the serpentine channel.

The microstructure of the semi-solid Al-20%Si alloy slurry, corresponding to four different pouring temperatures, is shown in Fig. 6(a), (b), (c) and (d). The as-solidified microstructure of all the Al-Si alloy specimens was composed of two types of phases, i.e., the dendritic Al-Si eutectic phase and the granular primary Si phase. Most of the primary Si grains showed a coarse polygonal or lath-like shape when the pouring temperature was under a range of 731-746 °C, as shown in Fig. 6(a) and (b). As the pouring temperature decreased to 716 °C, the number of fine granular primary Si grains increased, as shown in Fig. 6(c). Figure 6(d) shows that the fine granular grains dominated the primary Si phase. The size of the primary Si grains decreased gradually with decreasing the pouring temperatures. The equivalent diameter of the primary Si was measured, and the corresponding statistical data are plotted in Fig. 7. For the alloy I and II, the proportion of the primary Si in the diameter range of 20-40 μm exceeded 50%. However, the diameter of the primary Si in the alloy III and IV mainly lay in the range of 10-30 μm.

Plotting the average equivalent diameter and the shape coefficient to the pouring temperature, could be established, as shown in Fig. 8(a). The error bars in the graphs were the variances of the equivalent diameters and the shape coefficients measured in different views. As the pouring temperature decreased from 746 to 701 °C, the average equivalent diameter decreased from 40.6 to 21.2 μm, and the shape coefficient

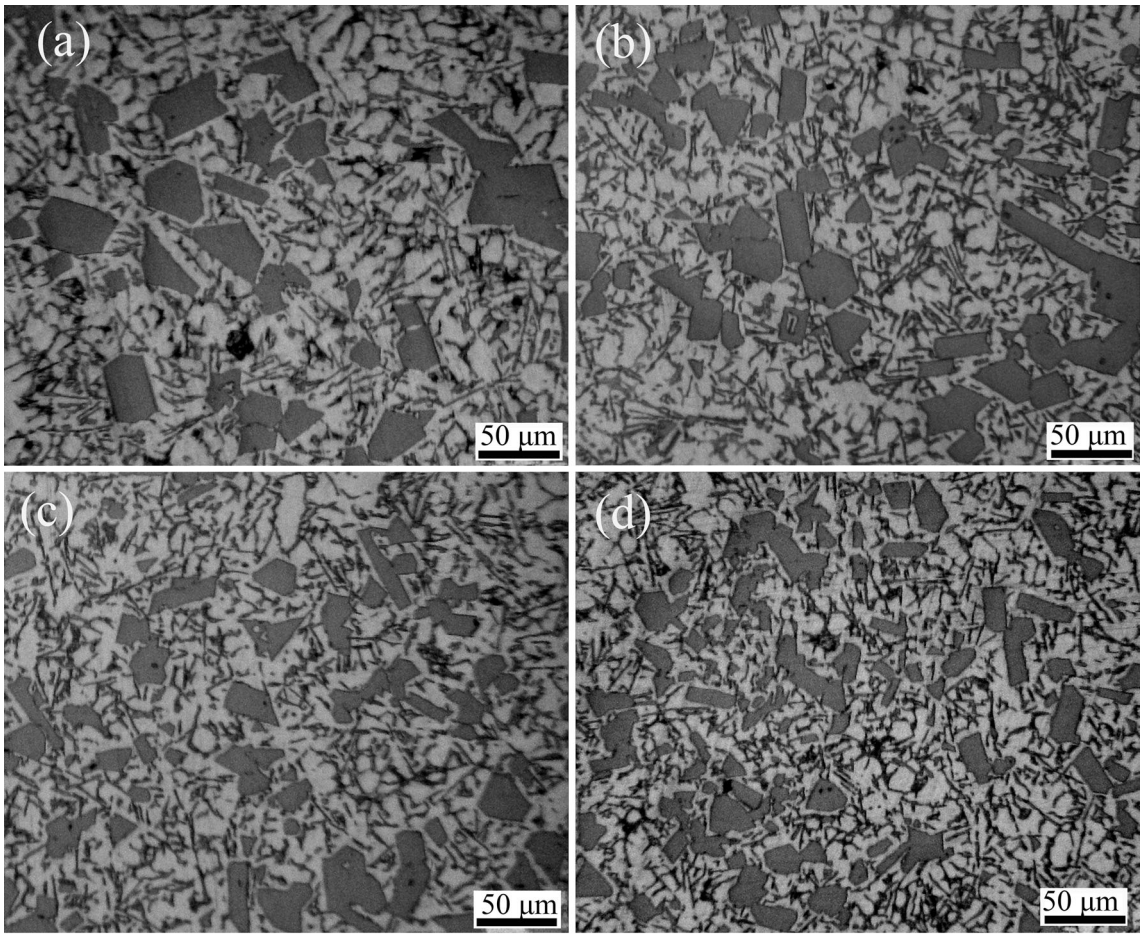

Fig. 6 Microstructures of the Al-20%Si alloy prepared by the serpentine channel with spoiler under different pouring temperatures, (a) Alloy I, (b) Alloy II, (c) Alloy III, (d) Alloy IV

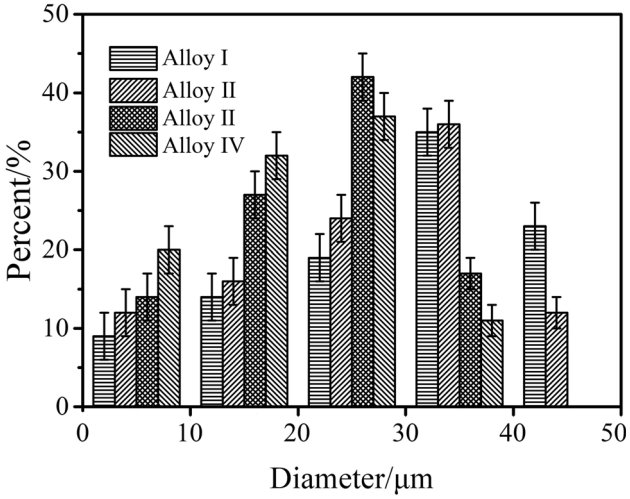

Fig. 7 The distribution of equivalent diameter of primary Si under different pouring temperatures

increased from 0.73 to 0.83. Tensile tests were carried out to evaluate the effect of the pouring temperature on the mechanical properties of the Al-20%Si alloy slurry. The average peak load of the three replicates for the alloy prepared at the same pouring temperature is presented in Fig. 8(b). The tensile strength increased from 252 to 298 MPa and the elongation increased from 8.4% to 11.6%, as the pouring temperature decreased from 746 to 701°C.

Figure 9 shows the SEM fracture morphologies of the tension test specimens. All the tension specimens experienced a mixed ductile-brittle fracture. The fracture surface of the tension specimen without the spoilers at 701 °C was covered by irregular cleavage planes and surrounding equiaxed dimples, as shown in Fig. 9(a). According to the EDS analysis at A zone, the cleavage plane was mainly composed of the primary Si. In addition, a small number of cracks could be identified on the cleavage planes. When introducing the spoilers at the same pouring temperature (Fig. 9b), the fine cleavage planes uniformly distributed on the fracture, and the cracks on the cleavage planes were substantially missing. As the pouring temperature increased from 701 to 746 °C, the size of the cleavage planes and the number of the cracks gradually increased, as illustrated in Fig. 9(b), (c), (d) and (e).

4. Discussion

The primary Si grains could be observed in the semi-solid Al-20%Si alloy slurry. The generation of the primary Si grains arose from the nucleation and growth of the Si phase in the alloy slurry. Under the pouring process of the semi-solid slurry,

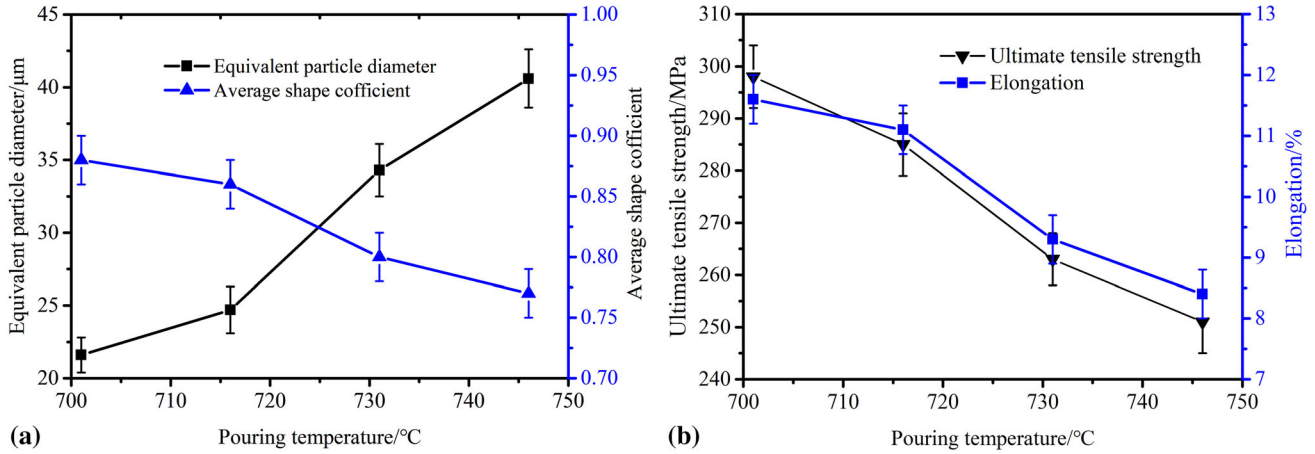

Fig. 8 Effect of the pouring temperature on the microstructure and mechanical property of the Al-20%Si alloy with the spoilers, (a) the average equivalent diameter and shape coefficient of the primary Si, (b) the ultimate tensile strength and elongation of the Al-20Si alloy

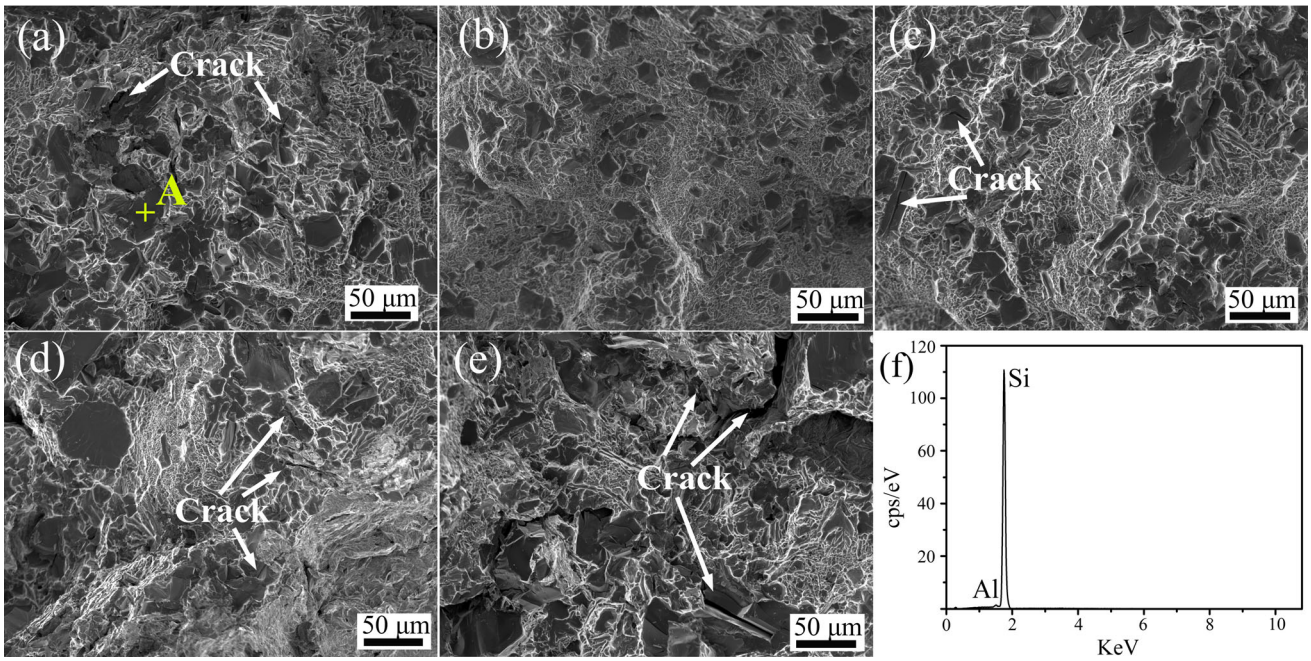

Fig. 9 Fracture morphologies of Al-20%Si alloy fabricated by the serpentine channel, (a) without the spoilers at 701 °C, with the spoilers at 701 °C (b), 716 °C (c), 731 °C (d) and 746 °C (e), (f) EDS analysis result of zone A

supercooling provided a thermodynamic condition for the nucleation of the primary Si in the alloy slurry (Ref 22, 23). As the slurry was directly poured into crucible, the supercooling degree of the slurry was quite low, which produced few nucleation points and coarse grains in the slurry. Different heat dissipation rates in all directions caused the dissimilar supercooling degrees during the slurry solidification (Ref 24). Thus, the primary Si in Fig. 3(a) exhibited a typical faceted character with a polygonal or lath-like structure. It has been reported that the morphology of the primary Si grains in the Al-Si alloy slurry could be changed from faceted to non-faceted pattern when the alloy slurry was deeply undercooled (Ref 25, 26). The serpentine channel wall improved the cooling rate of the alloy slurry, and enhanced its supercooling degree. Besides, the serpentine channel inner wall diminished the required interface energy during nucleation, and the primary Si could nucleate at a low supercooling degree. Thus, the primary Si grains in the Al-20%Si alloy prepared through the serpentine channel exhibited small size and a non-faceted shape.

A low pouring temperature caused a wide semi-solid temperature range in the serpentine channel (Table 2), which might strengthen the refining effect of the spoiler on the primary Si. Thus, it is firstly necessary to verify the effect of the spoiler on the alloy slurry at a pouring temperature of 701 °C. The introduction of the spoiler had little influence on the distribution uniformity of the primary Si grains in the Al-20%Si alloy, but the size of the primary Si grains changed. The average equivalent diameter of the primary Si grains was 21.2 μm, which was less than that of grains prepared without the spoiler (Fig. 4). The stirring force in the alloy slurry induced the uncoupled movement between the primary phase and surrounding liquids, which had a positive effect on the primary

phase refinement (Ref 9). In order to further understand the effect of the spoiler on the alloy slurry, the ANSYS software was employed to simulate the flow of the slurry in the serpentine channel. The transverse perspective velocity diagrams of the fluid flow are displayed in Fig. 10. The flow velocity and direction of the slurry could be observed directly. The velocity at the bends was greater than that at the straight channel, which indicated the stirring effect of the bends on the alloy slurry (Ref 10). For the serpentine channel with the spoiler, the flow direction of the slurry below the spoilers was disorganized, which implied the strong stirring effect of the spoiler on the alloy slurry. The superimposed stirring effects of the bend and spoiler on the alloy slurry increased the fragmentation probability of the primary Si grains, and further refined the primary Si grains. According to the Griffith equation, the fine primary Si grains has less internal defects than the coarse grains (Ref 27). Thus, few cracks appeared on the fine cleavage plane of the fracture (Fig. 9b), which was beneficial to the tensile properties of the specimens. Besides, it was reported that the tensile strength and elongation of the hypereutectic Al-Si alloy increased with decreasing the primary Si size (Ref 28, 29). Thus, the tensile strength and elongation of the Al-20%Si alloy prepared with the spoiler were larger than that prepared without the spoilers (Fig. 5).

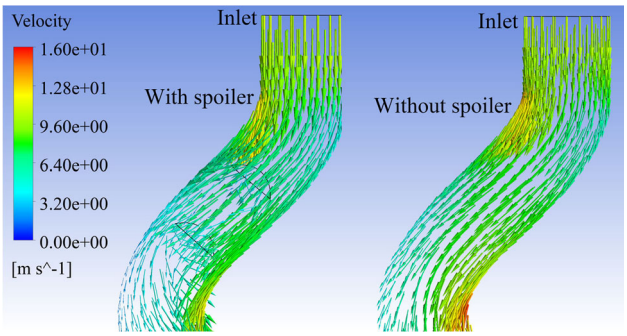

Fig. 10 Simulated velocity diagram of the fluid flow during the alloy slurry preparation

As is shown in Fig. 11, one grain was employed to demonstrate the evolution process of the primary Si grains in the serpentine channel. Firstly, the grain nucleated and grew in the straight channel without the spoilers, as marked by "I" part (Fig. 11a and b). Secondly, the grain was fragmented by the bend wall, as marked by "II" part (Fig. 11a and c). Finally, the fragmented grain continued to grow in the next straight channel, as marked by "III" part (Fig. 11a and d). After introducing the spoilers, the grain would be fragmented again by the spoilers at the straight channel. Thus, the primary Si grains in the serpentine channel with the spoilers remained a small size throughout the pouring process (Fig. 11e, f, g and h).

The pouring temperature was a critical parameter for the refinement of the primary Si in the semi-solid Al-Si alloy slurry (Ref 30, 31). A low pouring temperature always caused a large supercooling degree in the semi-solid alloy slurry, which accelerated the nucleation of the primary Si (Ref 31). Besides, the primary Si in the semi-solid slurry had no enough time to grow at a low pouring temperature (Ref 32). Thus, the size of the primary Si grains in the semi-solid alloy slurry decreased gradually with decreasing the pouring temperature from 746 to 701 °C (Fig. 6). The hard primary Si particles blocked the dislocation motion in the Al matrix, and increased the deformation resistance of the Al-Si alloy. The cracks always initiated at the hard Si particles when the resistance continued to grow. A large number of fine primary Si grains would result in great resistance to matrix deformation (Ref 33). Thus, as the decrement of the primary Si size, the tensile properties of the specimens increased, and the size of the cleavage plane on the fracture decreased (Fig. 9b, c, d and e). This result was consistent with previous research (Ref 34).

For comparison, a 'size-decrease-ratio' was defined as $(D_0 - D_1)/D_0$, where D_1 and D_0 are the equivalent diameters of the primary Si grains after and before grain refinement in the hypereutectic Al-Si alloy, respectively. Several size-decrease-ratios of primary Si grains with various preparation technologies are plotted in Fig. 12. The maximum size-decrease-ratio was obtained for the Al-Si alloy prepared with Nb inoculation. However, the Nb addition made the Al alloy's mechanical properties complicated (Ref 35). The serpentine channel with the spoilers caused a high size-decrease-ratio, which demonstrated its superior performance to the electromagnetic stirring

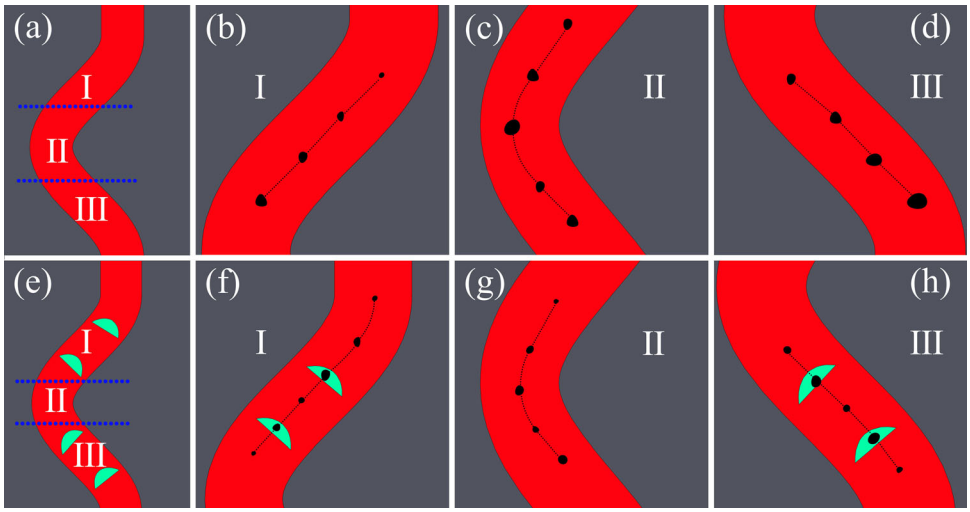

Fig. 11 The evolution process of the primary Si grains in the serpentine channel, (a-d) without the spoilers, (e-h) with the spoilers

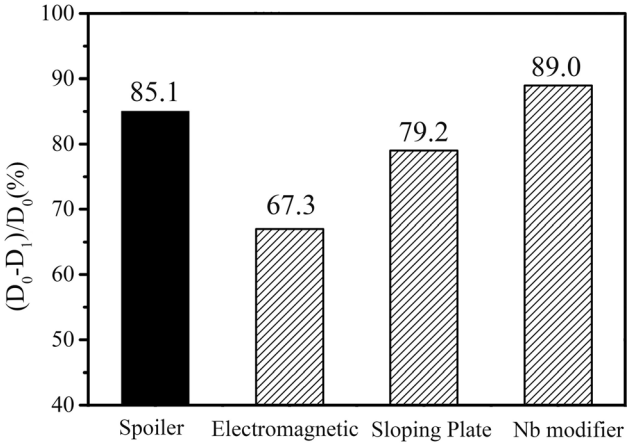

Fig. 12 The size-decrease-ratio of the primary Si in the hypereutectic Al-Si alloy prepared by various preparation technologies

(Ref 9) and wavelike sloping plate rheocasting (Ref 11). Therefore, the serpentine channel with the spoilers is a competitive method to refine the size of the primary Si in the hypereutectic Al-Si alloy. In addition, it was emphasized that the pouring temperature range of 686-701 °C could be further optimized by reducing the temperature interval. This means that the size of the primary Si could continue to be refined. Apart from the pouring temperature studied here, the serpentine channel structure (i.e., spoiler size, channel material and diameter) is also a critical issue, and can greatly influence the optimum pouring temperature and productivity of the semi-solid Al-Si alloy slurry. Our future work will be concentrated on this issue.

5. Conclusions

(1) The semi-solid Al-20%Si alloy slurry could be prepared by the serpentine channel with the spoilers, and the microstructure of the alloy slurry was composed of the primary Si and Al-Si eutectic phases.
(2) The spoilers had a significant effect on refining the primary Si grains in the Al-20%Si alloy slurry. The average equivalent diameter of the primary Si grains in the Al-20%Si alloy could be reduced to 21.2 μm, and the average shape coefficient could be increased to 0.83 under this experimental condition.
(3) The tensile strength and elongation of the Al-20%Si prepared with the spoilers were greater than those of the alloy prepared without the spoilers. As the pouring temperature decreasing from 746 to 701 °C, the tensile strength of the alloy increased from 252 to 298 MPa, and the elongation increased from 8.4 to 11.6%.

Acknowledgment

This work was supported financially by the Scientific and Technological Project of Henan Province (212102210350), the Research Foundation for Advanced Talents of Henan University of Technology (2019BS052), and Henan Province science and technology research project (222102220018).

References

1. R. Haghayeghi and G. Timelli, An Investigation on Primary Si Refinement by Sr and Sb Additions in a Hypereutectic Al-Si Alloy, *Mater. Lett.*, 2021, **283**, p 128779.
2. G.L. Mao, H. Yan, C.C. Zhu, Z. Wu, and W.L. Gao, The Varied Mechanisms of Yttrium (Y) Modifying a Hypoeutectic Al-Si Alloy Under Conditions of Different Cooling Rates, *J. Alloy. Compd.*, 2019, **806**, p 909–916.
3. X.Z. Zhu, S.H. Wang, X.X. Dong, X.F. Liu, and S.X. Ji, Morphologically Templated Nucleation of Primary Si on AlP in Hypereutectic Al-Si Alloys, *J. Mater. Sci. Technol.*, 2022, **100**, p 36–45.
4. E. Damavandi, S. Nourouzi, S.M. Rabiee, R. Jamaati, A.A. Tiamiyu, and J.A. Szpunar, Effects of Prior ECAP Process on the Dynamic Impact Behaviors of Hypereutectic Al-Si Alloy, *Mater. Sci. Eng. A-Struct.*, 2020, **793**, p 139902.
5. H.R. Kotadia, G. Gibbons, A. Das, and P.D. Howes, A Review of Laser Powder Bed Fusion Additive Manufacturing of Aluminium Alloys: Microstructure and Properties, *Addit. Manuf.*, 2021, **46**, p 102155.
6. Y.K. Li, S.Y. Xi, G.D. Ma, Y. Xiao, L. Li, Z.T. Yuan, Y.H. He, R.F. Zhou, and Y.H. Jiang, Understanding the Influencing Mechanism of Sub-Micron Sized TiB2p on the Microstructures and Properties of Rheological Squeeze Casting Hypereutectic Al–Si Alloys, *J. Mater. Res. Technol.*, 2021, **14**, p 57–68.
7. C. Sumalatha, P.V.C.S. Rao, V.V.S. Rao, and M.S.K. Deepak, Influence of Grain Refiner, Modifier and Graphene on the Dry Sliding Wear of Hypereutectic Al-Si Alloys, *Metallogr. Microstruct.*, 2022, **11**(2), p 234–244.
8. Y.J. Xu, Y. Deng, D. Casari, R.H. Mathiesen, X.F. Liu, and Y.J. Li, Revealing the Nucleation Kinetics of Primary Si Particles in Hypereutectic Al-Si Alloys Under the Influence of P Inoculation, *J. Mater. Sci.*, 2020, **55**(32), p 15621–15635.
9. M.J. Li, N.K. Omura, Y. Murakami, I. Matsui, and S.J. Tada, A Comparative Study of the Primary Phase Formation in Al-7 wt% Si and Al-17 wt% Si Alloys Solidified by Electromagnetic Stirring Processing, *Mater. Today. Commun.*, 2020, **24**, p 101146.
10. W.Z. Yu, Y. Xue, J. Mei, X.Z. Zhou, M.L. Xiong, and S.F. Zhang, Segregation and Removal of Transition Metal Impurities During the Directional Solidification Refining of Silicon with Al-Si Solvent, *J. Alloy. Compd.*, 2019, **805**, p 198–204.
11. R.G. Guan, Z.Y. Zhao, C.S. Lee, Q.S. Zhang, and C.M. Liu, Effect of Wavelike Sloping Plate Rheocasting on Microstructures of Hypereutectic Al-18 pct Si-5 pct Fe Alloys, *Metall. Mater. Trans. B*, 2012, **43**(2), p 337–343.
12. D.K. Yadav and I. Chakrabarty, Effect of Cooling Slope Casting and Partial Remelting Treatment on Microstructure and Mechanical Properties of A319-xMg2Si In-Situ Composites, *Mat. Sci. Eng. A-Struct.*, 2020, **791**, p 139790.
13. P. Das, S.K. Samanta, R. Das, and P. Dutta, Optimization of Degree of Sphericity of Primary Phase During Cooling Slope Casting of A356 Al Alloy: Taguchi Method and Regression Analysis, *Measurement*, 2014, **55**, p 605–615.
14. L.W. Chen, J. Li, W.P. Chen, X.L. Pei, H. Hou, and Y.H. Zhao, Comprehensive Assessment and Multiple-Response Optimization of Serpentine Channel Pouring Process for Achieving High-Quality Semi-Solid Slurry, *J. Mater. Res. Technol.*, 2023, **24**, p 3839–3852.
15. L.W. Chen, Y.H. Zhao, F. Yan, and H. Hou, Statistical Investigations of Serpentine Channel Pouring Process Parameters on Semi-Solid ZL101 Aluminum Alloy slurry using response surface Methodology, *J. Alloy. Compd.*, 2017, **725**, p 673–683.
16. Z.K. Zheng, Y.J. Ji, W.M. Mao, R. Yue, and Z.Y. Liu, Influence of Rheo-Diecasting Processing Parameters on Microstructure and Mechanical Properties of Hypereutectic Al-30% Si Alloy, *Trans. Nonferrous Metal. Soc.*, 2017, **27**(6), p 1264–1272.
17. Z.K. Zheng, W.M. Mao, Z.Y. Liu, D. Wang, and R. Yue, Refinement of primary Si grains in Al-20%Si alloy slurry through serpentine channel pouring process, *Int. J. Min. Met. Mater.*, 2016, **23**(5), p 572–580.

18. P.Y. Yan, W.M. Mao, J. Fan, B.K. Wang, and Y.B. Liu, Microstructural Evolution, Segregation and Fracture Behavior of A390 Alloy Prepared by Combined Rheo-HPDC Processing and Sr-Modifier, *J. Alloy. Compd.*, 2020, **835**, p 155297.
19. Z.Y. Liu, W.M. Mao, T. Wan, G.T. Cui, and W.P. Wang, Study on Semi-Solid A380 Aluminum Alloy Slurry Prepared by Water-Cooling Serpentine Channel and Its Rheo-Diecasting, *Met. Mater. Int.*, 2021, **27**(7), p 2067–2077.
20. S. O'Regan, P.J. Frawley, and O. Shardt, The Effects of Particle Shape, Orientation, and Reynolds Number on Particle-Wall Collisions, *Comput. Fluids*, 2023, **266**, p 106053.
21. Y. Bao and H. Wang, Numerical Study on Flow and Heat Transfer Characteristics of a Novel Tesla Valve with Improved Evaluation Method, *Int. J. Heat Mass Tran.*, 2022, **187**, p 122540.
22. I. Shamseddine, F. Pennec, P. Biwole, and F. Fardoun, Supercooling of Phase Change Materials: A Review, *Renew. Sust. Energ. Rev.*, 2022, **158**, p 112172.
23. B. Zhou, Z.Y. Qiu, K.P. Chen, C. Xu, and Z.Y. Wang, Microstructure Properties, and Numerical Simulation of Semi-Solid Aluminum Alloy under Planetary Stirring Process, *Materials*, 2022, **15**(9), p 3009.
24. P. Jin, Y.B. Liu, and Q.J. Sun, Evolution of Crystallographic Orientation, Columnar to Equiaxed Transformation and Mechanical Properties Realized by Adding TiCps in Wire and Arc Additive Manufacturing 2219 Aluminum Alloy, *Addit. Manuf.*, 2021, **39**, p 101878.
25. T. Aoyama and K. Kuribayashi, Influence of Undercooling on Solid/Liquid Interface Morphology in Semiconductors, *Acta Mater.*, 2000, **48**(14), p 3739–3744.
26. C.Y. Tan, M.A.A.M. Salleh, X.F. Tan, H. Yasuda, N. Saud, M.I.I. Ramli, and K. Nogita, Properties of Sn-3 wt%Ag-5 wt%Cu Alloys with Cu6Sn5 Intermetallics Grain Refined by Mg, *Mater. Today. Commun.*, 2022, **31**, p 103221.
27. C. Xu, H. Wang, Y. Yang, and Q. Jiang, Effect of Al-P-Ti-TiC-Nd_2O_3 Modifier on the Microstructure and Mechanical Properties of Hypereutectic Al-20wt.%Si Alloy, *Mater. Sci. Eng. A*, 2007, **452**, p 341–346.
28. R. Haghayeghi, L.C. Paula, and E.J. Zoqui, Comparison of Si Refinement Efficiency of Electromagnetic Stirring and Ultrasonic Treatment for a Hypereutectic Al-Si Alloy, *J. Mater. Eng. Perform.*, 2017, **26**, p 1900–1907.
29. M.H. Abdelaziz, A.M. Samuel, H.W. Doty, S. Valtierra, and F.H. Samuel, Effect of Additives on the Microstructure and Tensile Properties of Al-Si Alloys, *J. Mater. Res. Technol.*, 2019, **8**(2), p 2255–2268.
30. G.D. Niu, Y. Wang, L.J. Zhu, J.W. Ye, and J. Mao, Fluidity of Casting Al-Si Series Alloys for Automotive Light-Weighting: A Systematic Review, *Mater. Sci. Tech-Lond.*, 2022, **38**(13), p 902–911.
31. X. Zhang, H. Xu, T. Chen, C.S. Wang, Y.L. Wang, L.J. Xu, and H.W. Li, Forming Properties and Microstructure of Al-Cu Alloy Prepared by Liquid-Die Forging, *J. Cent. South. Univ.*, 2022, **29**(1), p 60–79.
32. M. Li, Y.D. Li, and H.W. Zhou, Effects of Pouring Temperature on Microstructure and Mechanical Properties of the A356 Aluminum Alloy Diecastings, *Mat. Res.*, 2020, **23**(1), p e20190676.
33. M. Li, N. Omura, Y. Murakami, I. Matsui, and S. Tada, A Comparative Study of the Primary Phase Formation in Al-7 wt% Si and Al-17 wt% Si Alloys Solidified by Electromagnetic Stirring Processing, *Mater. Today Commun.*, 2020, **24**, p 101146.
34. M.M. Shehata, S. El-Hadad, M.E. Moussa, and M. El-Shennawy, Optimizing the Pouring Temperature for Semisolid Casting of a Hypereutectic Al–Si Alloy Using the Cooling Slope Plate Method, *Int. J. Metalcast.*, 2021, **15**, p 488–499.
35. M. Nowak, L. Bolzoni, and N.H. Babu, The Effect of Nb-B Inoculation on Binary Hypereutectic and Near-Eutectic LM13 Al-Si Cast Alloys, *J. Alloy. Compd.*, 2015, **641**, p 22–29.